



Manipulation of Host Hepatocytes by the Malaria Parasite for Delivery into Liver Sinusoids

Angelika Sturm, *et al.*
Science **313**, 1287 (2006);
DOI: 10.1126/science.1129720

The following resources related to this article are available online at www.sciencemag.org (this information is current as of February 20, 2009):

Updated information and services, including high-resolution figures, can be found in the online version of this article at:

<http://www.sciencemag.org/cgi/content/full/313/5791/1287>

Supporting Online Material can be found at:

<http://www.sciencemag.org/cgi/content/full/1129720/DC1>

A list of selected additional articles on the Science Web sites **related to this article** can be found at:

<http://www.sciencemag.org/cgi/content/full/313/5791/1287#related-content>

This article **cites 12 articles**, 4 of which can be accessed for free:

<http://www.sciencemag.org/cgi/content/full/313/5791/1287#otherarticles>

This article has been **cited by** 30 article(s) on the ISI Web of Science.

This article has been **cited by** 3 articles hosted by HighWire Press; see:

<http://www.sciencemag.org/cgi/content/full/313/5791/1287#otherarticles>

This article appears in the following **subject collections**:

Microbiology

<http://www.sciencemag.org/cgi/collection/microbio>

Information about obtaining **reprints** of this article or about obtaining **permission to reproduce this article** in whole or in part can be found at:

<http://www.sciencemag.org/about/permissions.dtl>

Manipulation of Host Hepatocytes by the Malaria Parasite for Delivery into Liver Sinusoids

Angelika Sturm,^{1*} Rogerio Amino,^{2,3*} Claudia van de Sand,¹ Tommy Regen,¹ Silke Retzlaff,¹ Annika Renneberg,¹ Andreas Krueger,¹ Jörg-Matthias Pollok,⁴ Robert Menard,² Volker T. Heussler^{1†}

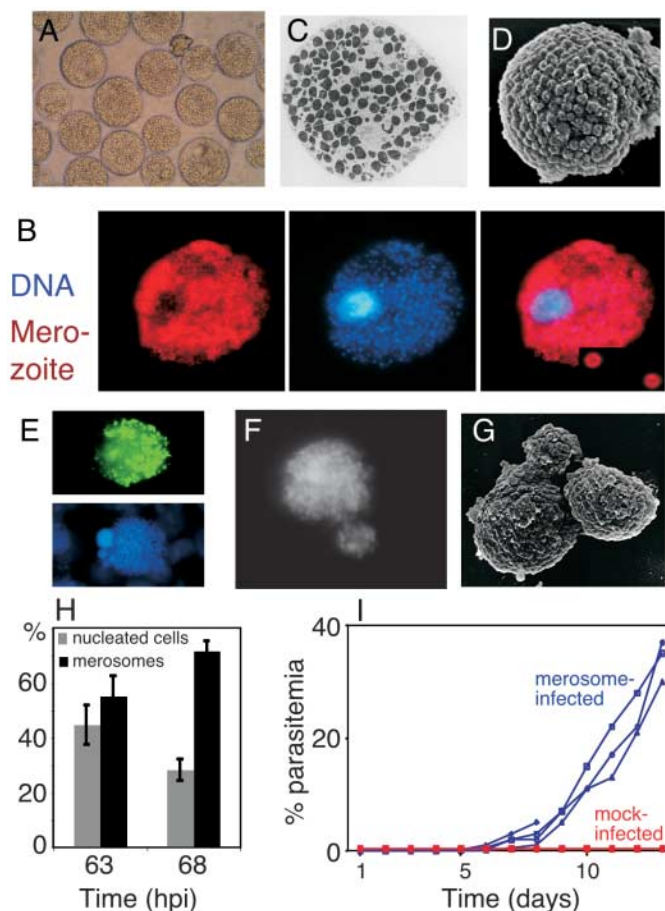
The merozoite stage of the malaria parasite that infects erythrocytes and causes the symptoms of the disease is initially formed inside host hepatocytes. However, the mechanism by which hepatic merozoites reach blood vessels (sinusoids) in the liver and escape the host immune system before invading erythrocytes remains unknown. Here, we show that parasites induce the death and the detachment of their host hepatocytes, followed by the budding of parasite-filled vesicles (merosomes) into the sinusoid lumen. Parasites simultaneously inhibit the exposure of phosphatidylserine on the outer leaflet of host plasma membranes, which act as “eat me” signals to phagocytes. Thus, the hepatocyte-derived merosomes appear to ensure both the migration of parasites into the bloodstream and their protection from host immunity.

Infection of a mammalian host by the malaria parasite starts when the sporozoite stage delivered by the mosquito reaches the liver and invades hepatocytes (1, 2). The intracellular sporozoite then differentiates and generates a new invasive and motile form, called the merozoite, which invades erythrocytes. To gain access to erythrocytes, the hepatic merozoite must reach the lumen of the liver sinusoids from hepatocytes through the space of Disse, a layer of extracellular matrix, and the sinusoid endothelium. It is not known how hepatic merozoites reach the blood and avoid phagocytosis by the numerous resident macrophages, called Kupffer cells, which patrol the liver sinusoids.

To address this issue, we first analyzed the terminal phase of parasite development inside hepatocytes in vitro. The complete development of *Plasmodium berghei*, a species that infects rodents, lasts 2 to 3 days in cultured hepatoma cells and in primary mouse hepatocytes. The process takes place inside a parasitophorous vacuole, which is formed upon parasite entry into the host cell, and involves the differentiation of a sporozoite into a large multinucleated schizont and eventually several thousands of merozoites. We first examined *P. berghei* maturation in vitro after incubation of sporozoites with the HepG2 hepatoma cell line. At 48 hours postinfection (hpi), parasites developed inside adher-

ent HepG2 cells as exo-erythrocytic forms (EEFs) (fig. S1). However, at 63 to 70 hpi, the number of adherent cells containing parasites

Fig. 1. Detached infected cells extrude merosomes, which contain infective merozoites. **(A)** Phase contrast image of infected HepG2 cells floating in the culture medium. **(B)** Immunofluorescence staining of a single floating cell with merozoite-specific antiserum (red); DNA is stained in blue (Hoechst 33258). Inset shows released merozoites at a higher magnification. **(C and D)** TEM and SEM of a single detached cell. **(E)** Disruption of the PVM during parasite merogony; green, Exp1; blue, Hoechst 33258. **(F)** Immunofluorescence image of living GFP-expressing parasites in a detached cell, demonstrating the budding of parasite-filled vesicles (merosomes). **(G)** SEM image of budding merosomes. **(H)** Merosome formation increases with time. Detached cells were collected after the indicated times, immobilized on poly-L lysine slides, fixed, and stained with the DNA dye Hoechst 33258. Nucleated cells and merosomes (devoid of host cell nucleus) were counted and the percentage (mean \pm SD) of both populations was calculated from three independent experiments. **(I)** Infection of mice with detached cells. Four mice received culture supernatant containing 20 to 50 detached cells/merosomes (blue lines). Four control mice (red lines) received an equal amount of culture supernatant without detached cells, to exclude the possibility that previously liberated merozoites caused infection.



¹Bernhard Nocht Institute for Tropical Medicine, Bernhard-Nocht-Strasse 74, 20359 Hamburg, Germany. ²Department of Parasitology, Institut Pasteur, 28 Rue du Dr. Roux, 75724 Paris Cedex 15, France. ³Department of Biochemistry, Federal University of Sao Paulo, Rua Tres de Maio, 04044-020, Sao Paulo, Brazil. ⁴Department of Hepatobiliary Surgery, University Hospital Hamburg-Eppendorf, Martinistrasse 52, 20246 Hamburg, Germany.

*These authors contributed equally to this work.

†To whom correspondence should be addressed. E-mail: heussler@bni-hamburg.de

declined sharply to \sim 40% of their initial number, although the culture supernatants contained only small numbers of free merozoites that would be expected from rupturing of these cells. Instead, large numbers of parasite-filled, floating cells were observed (Fig. 1, A and B). Examination of these detached infected cells by transmission electron microscopy (TEM) (Fig. 1C and fig. S2) and scanning electron microscopy (SEM) (Fig. 1D) confirmed the presence of normal-shaped merozoites filling the whole volume of the host cells. The pattern of immunofluorescence staining (3) with polyclonal antibodies specific for the exported protein 1 (Exp1), a parasite protein that becomes inserted into the parasitophorous vacuole membrane (PVM), indicated disruption of the PVM (Fig. 1E) and liberation of merozoites into the host cell cytoplasm.

Unexpectedly, merozoites were also found within round, membrane-bound vesicles that were devoid of host cell nuclei and that we named merosomes (Fig. 1, F and G). Merosomes of various sizes were formed upon budding from the detached host cells (Fig.

1H). To test whether merozoites inside detached cells and merosomes were infective, we injected them intravenously into mice. Parasites were detected in the blood of all injected mice (Fig. 1I), showing that the detached host cells could release infectious merozoites.

To examine if merosomes were also formed in vivo, we injected wild-type *P. berghei* sporozoites into C57/Bl6 mice and analyzed liver sections for the presence of detached infected cells and merosomes. At 40 hpi, most infected hepatocytes were still closely connected to neighboring hepatocytes (Fig. 2A, left), whereas at 46 hpi we detected predominantly detached cells, or parasite-filled cell extensions inside blood vessels (Fig. 2A, right). To obtain a real-time view of the process of merozoite release, we injected sporozoites from different *P. berghei* clones

that express the green fluorescent protein (GFP) (4, 5) into animals and monitored 45- to 53-hpi parasite-infected cells in the liver by time-lapse intravital imaging (3). EEFs appeared as large green fluorescent structures in the liver parenchyma. With time, however, fluorescent cell extensions, presumably corresponding to the merosomes seen in vitro, were observed budding from infected cells and reaching the blood circulation (Fig. 2, B to F, and movies S1 to S4). Based on the volume of individual merozoites and of released merosomes, it was estimated that merosomes can contain from just a few to several thousand merozoites. Once in the circulation, merosomes usually appeared to remain intact for extended periods of time (>1 hour) and drifted at a much slower speed than that of circulating erythrocytes, suggesting that the surface of

merosomes might interact with that of liver sinusoid endothelial cells.

The process of merosome release from mature EEFs in the liver was next quantified in two distinct mouse strains (total number of mice, $n = 8$). On average, the percentage of budding EEFs increased between 42 and 50 hpi from ~39 to ~52% (Fig. 2D, $n = 88$ EEFs). During this time, 56% of merosomes were located inside sinusoids (Fig. 2, E and F), confirming the results of the histological examinations (Fig. 2A). The EEFs that were not seen emitting merosomes during the observation intervals were frequently still growing in size, suggesting that merosome budding might have followed the observation period. We conclude that merosome release from mature EEFs is a common phenomenon that occurs in most, if not all, mature *P. berghei* liver stages, and that merosomes can ensure

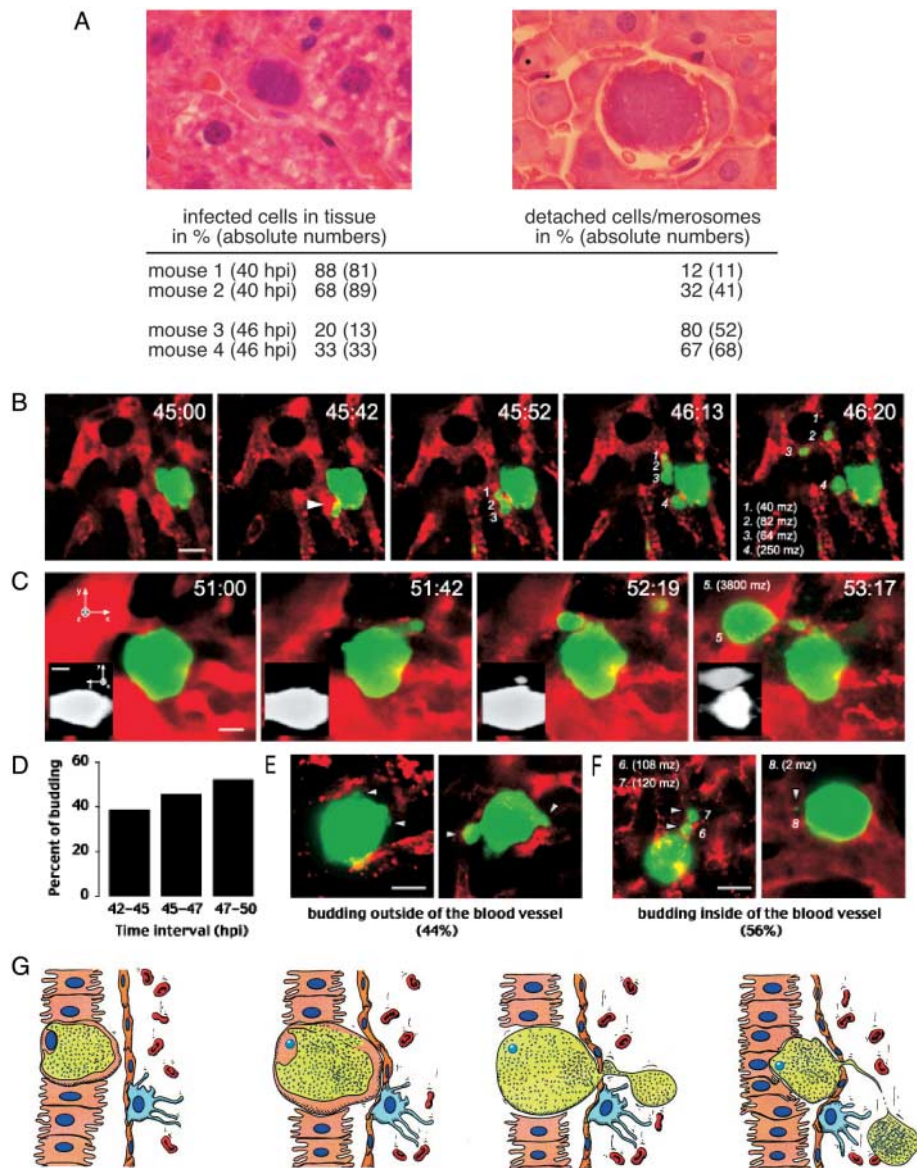


Fig. 2. Histological and real-time analysis of merozoite release in the liver of mice. (A) Histological sections showing EEFs at 40 to 46 hpi in the parenchyma (left) and in the sinusoids (right), respectively. Detached cells/merosomes and infected cells in the liver parenchyma of four different mice were counted and are presented as the percentage of infected cells counted (absolute numbers are in parentheses). (B to F) Intravital imaging of EEF budding and merosome release by confocal microscopy. The GFP-expressing parasite is shown in green and the blood circulation in red (red fluorescent bovine serum albumin injected intravenously). White arrowheads show host cell buds. The time postinfection (in hours) is shown in the upper-right corner. Bars, 15 μ m. (B) Time-lapse sequence showing a green fluorescent EEF budding merosomes inside a small sinusoid. The merosomes are labeled with a number, and the estimated number of merozoites (mz), calculated as the merosome volume divided by the merozoite volume (2.66 μ m³), is shown in parentheses. (C) Each panel of the colored time-lapse sequence is a maximum projection of three images covering 8 μ m in depth. The sequence shows a late EEF budding a large merosome, which is growing while moving toward the central vein. The insets show the EEF lateral view (90° counter-clockwise rotation of γ axis). As shown by the last two insets, the diameter of the blood vessel limits the size of the merosome and the transfer of merozoites from the EEF into the merosome. (D) Quantification of budding EEF in the liver of mice ($n = 88$ EEFs). (E and F) Percentage of parasites budding outside the nearby sinusoid versus those budding inside ($n = 46$ budding EEFs). The confocal images are representatives of each type of budding. (G) Hypothesis for the release of *Plasmodium* merozoite-filled vesicles (merosomes, green) from infected hepatocytes. Red blood cells (red) are separated from hepatocytes by endothelial cells (orange) and the space of Disse. Kupffer cell is in blue.

the direct delivery of merozoites in the blood circulation.

The molecular events during cell detachment and merozoite formation were next analyzed *in vitro*. Staining of the infected HepG2 cells early after detachment with the nucleic acid stain Hoechst 33258 revealed condensation of the cell nuclei, suggesting that these cells were undergoing cell death (Fig. 3A, lower panels). Loss of mitochondria membrane potential (fig. S3) and the release of cytochrome c from mitochondria of infected cells (Fig. 3A) supported this assumption. In agreement with these observations, electron microscopy showed that detached cells did not contain normal-shaped mitochondria (fig. S4). However, host cell death did not occur by classic apoptosis or necrosis (Fig. 3B and Fig. 4, A, B, and D). Activation of cysteine proteases other than caspases induced cell death (Fig. 3B). Treatment of infected HepG2 cells with the general cysteine protease inhibitor E64 at 55 hpi completely inhibited PVM destruction and cytochrome c release (fig. S5), and no detached cells were detected in the culture medium. When infected cultures were treated with E64 at 61 hpi (1 to 2 hours before infected cells normally detach), most infected cells did not detach, but a proportion of infected cells were still floating in the culture medium (Fig. 3B). These cells exhibited a different phenotype compared with that of untreated detached cells. The

PVM of E64-treated detached cells was still visible, and the host cell nucleus appeared less condensed than in untreated detached cells (Fig. 3C). Therefore, E64 appeared capable of blocking the ongoing processes of PVM and host cell nucleus destruction mediated by cysteine proteases. Other key differences between cell death observed in detached cells and apoptosis were that the DNA in condensed host cell nuclei was not fragmented (Fig. 4D and fig. S6) and that in the membrane of detached cells and merozoites, the asymmetric distribution of phosphatidylserine (PS) residues, which is normally a hallmark of viable cells, was maintained (Fig. 4, A and B, and fig. S7). The recognition of dead versus viable cells by phagocytes relies, at least in part, on exposure of PS on the outer leaflet of the membrane of dying cells (6–8), and we therefore analyzed how the parasite manipulates the host cell signaling machinery, resulting in the inhibition of the PS switch (3). In apoptotic cells, the PS switch is initiated by Ca^{2+} release from internal stores like mitochondria and the endoplasmic reticulum into the cytoplasm of the cell. Staining of detached, infected cells with a cell-permeable Ca^{2+} -indicator dye revealed that merozoites contained much higher levels of intracellular Ca^{2+} than host cells (Fig. 4B, upper panels). This suggests that like *P. falciparum* erythrocytic merozoites (9, 10), hepatic merozoites actively accumu-

late intracellular Ca^{2+} , which is released from damaged internal stores of the dying host cell. Ca^{2+} uptake by merozoites keeps Ca^{2+} levels in the host cell low and inhibits the PS switch to the outer leaflet of the host cell membrane as long as the intracellular parasites are viable. However, forced Ca^{2+} influx in detached cells by treatment with the Ca^{2+} ionophore ionomycin induced the PS switch, indicating that there is not a general block of PS exposure in these cells (Fig. 4A).

Under *in vitro* conditions, merozoites in detached hepatocytes have a restricted lifetime. Parasite death is accompanied by DNA fragmentation (Fig. 4D) and Ca^{2+} release from the parasite back into the host cell cytoplasm, resulting in PS switch to the outer leaflet of the host cell membrane (Fig. 4, A and B, lower panel). In phagocytosis assays, ionomycin-treated PS-positive detached cells were more frequently engulfed by macrophages than PS-negative detached cells containing viable parasites (fig. S8).

In marked contrast to the induction of cell death observed during merozoite development, it has recently been shown that early *Plasmodium* liver stages even confer resistance to apoptosis to the host cell (11, 12). However, dying EEFs were shown to provoke phagocyte infiltration *in vivo*, and it was suggested that these dead parasites cannot protect host cells from under-

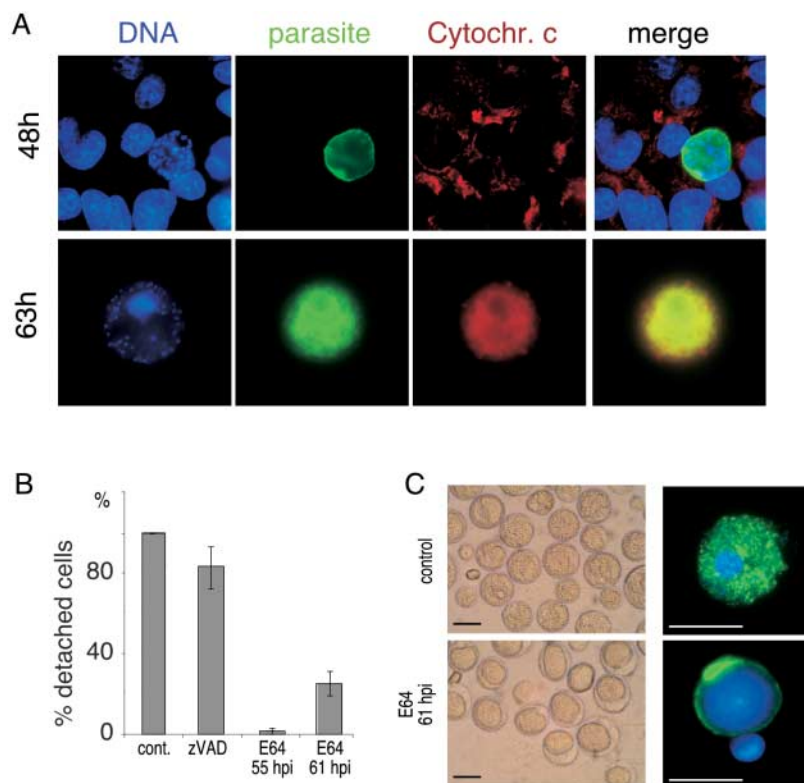


Fig. 3. Induction of host cell death during merozoite formation. (A) Cytochrome c release from mitochondria in floating cells. Infected HepG2 cells were fixed at 48 hpi (control, upper panels) or 63 hpi (lower panels) and stained with antibodies against PbExp1 or Pbhsp90 (green) and cytochrome c (red). (B) The general cysteine protease inhibitor E64, but not the caspase inhibitor zVAD-fmk, blocks the detachment of host cells. Cultures were left untreated (cont.) or treated with E64 at 55 or 61 hpi, or with zVAD-fmk (at 55 hpi). At 65 hpi, culture supernatants were collected and the number of floating cells was determined. Results are expressed as the percentage of control cells (mean \pm SD). (C) Cultures were treated with E64 at 61 hpi for 4 hours. Treated detached cells (lower panels) exhibit a different phenotype from that of untreated control cells (upper panels). Immunofluorescent analysis with an antibody against the PVM protein Exp1 (right panels) shows the partly preserved PVM in E64-treated cells (lower right panel). The structure of the PVM was maintained in 76% (\pm 12%) of detached cells treated with E64 from 61 to 65 hpi. DNA is stained with Hoechst 33258 (blue). Bars, 20 μ m.

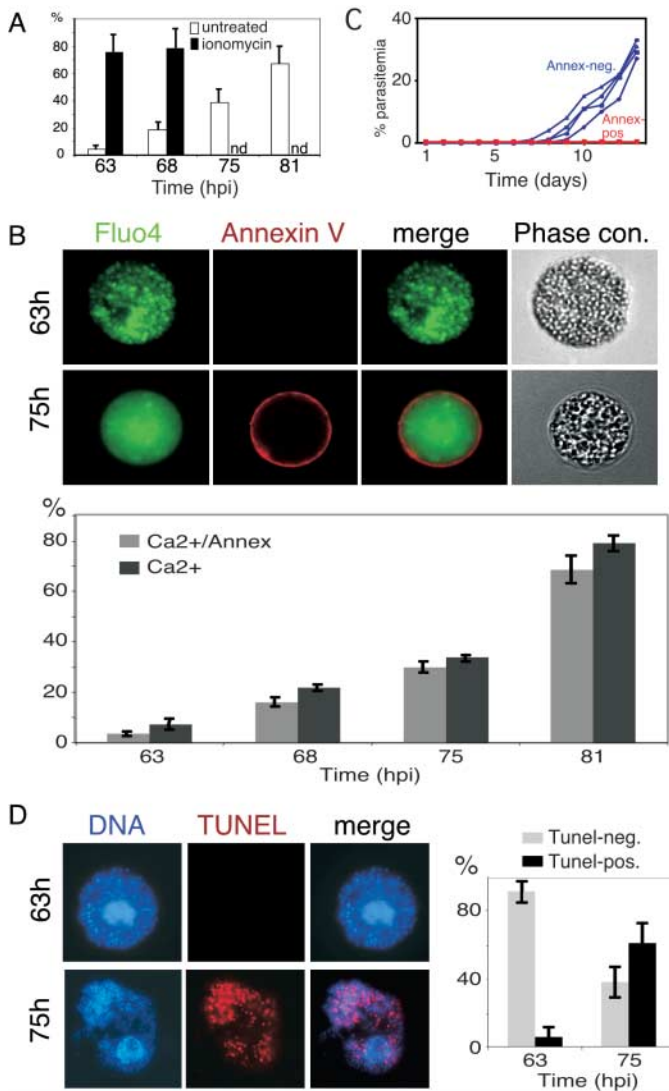


Fig. 4. Merosomes do not expose PS at their surface for several hours. **(A)** Detached cells were isolated at different time points and stained with Annexin-V—fluorescein isothiocyanate and propidium iodide (see also fig. S7). The percentage (mean \pm SD) of Annexin-V–positive cells was calculated from three independent experiments (white bars). Detached cells treated for 1 (63 hpi) and 6 hours (68 hpi) with ionomycin (1 μ g/ml) are represented by black bars (mean \pm SD; nd, not done). **(B)** Merozoites accumulate Ca^{2+} and inhibit the PS switch in the host cell membrane. Floating cells at 63 hpi (upper panels) and 75 hpi (middle panels) were stained with Fluo-4/AM (green) and Annexin-V-Alexa 568 (red). Quantitative assessment of Ca^{2+} release and PS switch (bottom panel). For each time point, 100 to 300 cells were examined and the percentage (mean \pm SD) of cells with released Ca^{2+} (dark bars) and cells with released Ca^{2+} and PS switch (gray bars) was calculated. **(C)** Detached, Annexin-V–stained cells at 63 or 75 hpi were isolated with a micropipette and transferred to 24-well plates; Annexin-V–positive or Annexin-V–negative floating cells were separated and subsequently injected into mice. Mouse parasitemia were determined daily for 2 weeks [four mice infected with Annexin-V–positive cells (red symbols); four mice infected with Annexin-V–negative cells (blue symbols)]. **(D)** TUNEL (terminal deoxynucleotidyl transferase–mediated dUTP nick-end labeling) staining of floating cells at 63 and 75 hpi. Red, TUNEL stain; blue, Hoechst 33258 stain. In three independent experiments, the total number of detached cells was determined and the number of TUNEL-positive cells was calculated and expressed as the percentage of all counted cells (mean \pm SD). Gray bars represent TUNEL-negative detached cells, black bars TUNEL-positive detached cells.

going cell death (12). The results obtained by intravital imaging indicate that the remnants of infected cells left behind after merosome release could also contribute to the observed phagocyte infiltration.

In conclusion, we have shown that *Plasmodium* liver-stage parasites manipulate their host cells to guarantee the safe delivery of merozoites into the bloodstream (Fig. 2G). Merosomes bulge into liver sinusoids and appear to act as shuttles that ensure the release of living merozoites directly into the circulation, and by not presenting the PS signature of a dying cell, also act as shields that protect them from phagocytosis. This mechanism of merozoite release may increase erythrocyte invasion and parasite survival, because extracellular merozoites are readily recognized and engulfed by Kupffer cells and other phagocytic cells in the liver sinusoids (13). The proteases that control cell death and cell movement of the host cell, as well as the factors that mediate Ca^{2+}

accumulation and prevent PS exposure, appear to be essential to parasite survival. They might become interesting targets for inhibiting the release of *Plasmodium* merozoites from hepatocytes and thus preventing erythrocyte infection and the onset of the disease.

References and Notes

1. U. Frevort *et al.*, *PLoS Biol.* **3**, e192 (2005).
2. R. Amino *et al.*, *Nat. Med.* **12**, 220 (2006).
3. Materials and methods are available as supporting material on Science Online.
4. R. Natarajan *et al.*, *Cell. Microbiol.* **3**, 371 (2001).
5. B. Franke-Fayard *et al.*, *Mol. Biochem. Parasitol.* **137**, 23 (2004).
6. B. Verhoven, R. A. Schlegel, P. Williamson, *J. Exp. Med.* **182**, 1597 (1995).
7. V. A. Fadok, A. de Cathelineau, D. L. Daleke, P. M. Henson, D. L. Bratton, *J. Biol. Chem.* **276**, 1071 (2001).
8. M. O. Li, M. R. Sarkisian, W. Z. Mehal, P. Rakic, R. A. Flavell, *Science* **302**, 1560 (2003).
9. M. Wasserman, J. P. Vernot, P. M. Mendoza, *Parasitol. Res.* **76**, 681 (1990).
10. G. A. Biagini, P. G. Bray, D. G. Spiller, M. R. White, S. A. Ward, *J. Biol. Chem.* **278**, 27910 (2003).

11. P. Leiriao *et al.*, *Cell. Microbiol.* **7**, 603 (2005).
12. C. van de Sand *et al.*, *Mol. Microbiol.* **58**, 731 (2005).
13. J. A. Terzakis, J. P. Vanderberg, D. Foley, S. Shustak, *J. Protozool.* **26**, 385 (1979).
14. We thank M. Lütgehetmann and S. Korton for technical advice and U. Froehle for technical assistance. We also thank C. Schmetz for electron microscopy imaging, S. Shorte for intravital imaging, and T. Ishino, M. Yuda, C. Janse, B. Franke-Fayard, and A. Waters for providing the *P. berghei* fluorescent clones. G. Langsley, E. Tannich, and H. Lotter are thanked for critically reading the manuscript. This work was supported by grant HE 4497/1-1 from the Deutsche Forschungsgemeinschaft (to V.T.H.) and a Howard Hughes Medical Institute International Scholar Award (to R.M.).

Supporting Online Material

www.sciencemag.org/cgi/content/full/1129720/DC1
 Materials and Methods
 Figs. S1 to S8
 Movies S1 to S4

9 May 2006; accepted 18 July 2006
 Published online 3 August 2006;
 10.1126/science.1129720
 Include this information when citing this paper.